Research Article

fMRI resting state time series causality: comparison of Granger causality and phase slope index

Ibrahim E. Hassan Saleh*

Department of Physics, Faculty of Science, Helwan University, Cairo, Egypt

ABSTRACT

Granger causality and Phase Slope Index (PSI) are recent approaches to measure how one signal depends on another, which gives an indication of information flow in complex systems. We show that the Granger causality and PSI mapping, voxel-by-voxel, for functional magnetic resonance imaging (fMRI) resting state data set. Slow fluctuations (< 0.1 Hz) in fMRI signal have been used to map several consistent resting state networks in the brain. The results demonstrate that PSI influence directions among reference regions and gray matter voxels were more consistent with the relevant previous studies compared with Granger causality. The PSI approach proposed is effective, computationally efficient, and easy to interpret.

Keywords: Granger causality, Phase Slope Index, fMRI resting state, Information flow

INTRODUCTION

Granger causality

Granger causality, proposed and formalized by C.W.J. GRANGER (1969) has been heavily criticised in the first years after the publication of his paper as it reduces causality to incremental predictability.[1] In time series analysis, this concept of causality is nevertheless widely accepted today. Granger (1969) defined causality as follow: A variable Y is causal for another variable X if knowledge of the past history of Y is useful for predicting the future state of X over and above knowledge of the past history of X itself. So if the prediction of X is improved by including Y as a predictor, then Y is said to be Grangercausal for X.

In functional neuroimaging, brain networks are primarily studied in terms of functional connectivity and effective connectivity. The most popular modeldriven approaches to study effective connectivity from fMRI data are structural equation modeling[2] and dynamic causal modelling.[3] These

techniques require a priori specification of an anatomical network model and are therefore best suited to make inferences on a limited number of possible networks. These disadvantages can largely be circumvented by Granger causality method, where recent work has begun to consider the causal influence one neural time series can exerts on another. The basic idea can be traced back to Wiener[4] who conceived the notion that, if the prediction of one time series could be improved by incorporating the knowledge of a second one, then the second series is said to have a causal influence on the first. Wiener's idea lacks the machinery for practical implementation. Granger later formalized the prediction idea in the context of linear regression models.[1]

There are several applications for Granger causality analysis in different fields, such as: economics,[5,6] bioinformatics,[7,8] geophysics,[9,10] and neuroscience.[11-13] With fMRI data, recent studies have interested to derive Granger causality maps by applied Granger causality analysis among a target region of interest and all other voxels in the brain[14-16] and applied a conditional Granger

causality analysis to evaluate the effective connectivity of resting state networks.[17,18]

Two additional developments of Granger's causality idea are important. First, for three or more simultaneous time series, the causal relation among any two of the series may be direct, may be mediated by a third one, or may be a combination of both. This situation can be addressed by the technique of conditional Granger causality. Second, natural time series, including ones from economics and neurobiology, contain oscillatory aspects in specific frequency bands. It is thus desirable to have a spectral representation of causal influence.

Pairwise Granger causality

If we have the two time series X and Y, the paired model is as following:

$$X_t = \sum_{j=1}^{P} a_{1j} X_{t-j} + \varepsilon_{1t} \qquad (1)$$

$$Y_t = \sum_{j=1}^{P} d_{1j} Y_{t-j} + \eta_{1t} \qquad (2)$$

The joint autoregressive representation for X_t and Y_t can be written as:

$$X_t = \sum_{j=1}^{P} a_{2j} X_{t-j} + \sum_{j=1}^{P} b_{2j} Y_{t-j} + \varepsilon_{2t} \qquad (3)$$

$$Y_t = \sum_{j=1}^{P} c_{2j} Y_{t-j} + \sum_{j=1}^{P} d_{2j} Y_{t-j} + \eta_{2t} \qquad (4)$$

Where X_t and Y_t represent the two time series at time t. X_{t-j} and Y_{t-j} represent the time series at time t-j, P represents the maximum number of lagged observations included in the model (the model order). ε_{1t} and ε_{2t} are the residuals (prediction errors) for each time series, and a, b, c and d are coefficients of the model for each time series. The noise covariance matrix can be represented as:

$$\Sigma 1 = \begin{pmatrix} var(\varepsilon_{2t}) & cov(\varepsilon_{2t}, \eta_{2t}) \\ cov(\eta_{2t}, \varepsilon_{2t}) & var(\eta_{2t}) \end{pmatrix} \qquad (5)$$

If a time series Y causes (or has an influence on) X, then knowledge of Y should help predict future values of X. Thus, causality (or influence) is framed in terms of predictability. In more detail, given two discrete time series X and Y, we say that Y Granger causes X if we can predict the current value of X, using past values of X and Y, better than we can when using past values of X alone. According to Wiener[4] and Granger[1] if var(ε_{2t}) is less than var(ε_{1t}) in some suitable statistical sense, then Y is said to have a causal influence on X. We quantify this causal influence from time series Y to X ($F_{Y \to X}$) by:

$$F_{Y \to X} = \ln \left(\frac{var(\varepsilon_{1t})}{var(\varepsilon_{2t})} \right) \qquad (6)$$

If $F_{Y \to X} = 0$, this mean that no further improvement in the predication of time series X can be expected by including past measurements of time series Y. If $F_{Y \to X} > 0$, there is causal influence from Y to X. Similarly, one can define causal influence from X to Y ($F_{X \to Y}$) as:

$$F_{X \to Y} = \ln \left(\frac{var(\eta_{1t})}{var(\eta_{2t})} \right) \qquad (7)$$

The instantaneous influence $F_{X.Y}$ quantifies the improvement in the prediction of the current value of X (or Y) by including the current value of Y (or X) in a linear model already containing the past values of X and Y. From this symmetry it can be seen that $F_{X.Y}$ indeed contains no directional information at all. The instantaneous indirect influence ($F_{X.Y}$) between time series X and time series Y is given as:

$$F_{X.Y} = \ln \left(\frac{var(\varepsilon_{2t}) var(\eta_{2t})}{|\Sigma 1|} \right) \qquad (8)$$

The influence measure $F_{X,Y}$ is the sum of three components: the directional causal influence from X to Y ($F_{X \to Y}$), the directional causal influence from Y to X ($F_{Y \to X}$), and the instantaneous influence between X and Y ($F_{X.Y}$).

$$F_{X,Y} = F_{X \to Y} + F_{Y \to X} + F_{X.Y} \qquad (9)$$

$F_{X,Y}$ is a measure of the total linear dependence between the series x and y.

Conditional Granger causality

Recently, the conditional Granger causality analysis has been applied to estimate functional coupling effectively in multivariate data sets.[19,20] Consider the case of three time series X_t, Y_t, and Z_t. First, the joint autoregressive representation for X_t and Z_t can be written as:

$$X_t = \sum_{j=1}^{P} a_{3j} X_{t-j} + \sum_{j=1}^{P} b_{3j} Z_{t-j} + \varepsilon_{3t} \qquad (10)$$

$$Z_t = \sum_{j=1}^{P} c_{3j} X_{t-j} + \sum_{j=1}^{P} d_{3j} Z_{t-j} + \gamma_{3t} \qquad (11)$$

and the noise covariance matrix can be represented as:

$$\Sigma 2 = \begin{pmatrix} var(\varepsilon_{3t}) & cov(\varepsilon_{3t}, \gamma_{3t}) \\ cov(\gamma_{3t}, \varepsilon_{3t}) & var(\gamma_{3t}) \end{pmatrix} \qquad (12)$$

Next, we consider the joint autoregressive representation for a system involving all the three time series X_t, Y_t and Z_t as:

$$X_t = \sum_{j=1}^{P} a_{4j} X_{t-j} + \sum_{j=1}^{P} b_{4j} Y_{t-j} + \sum_{j=1}^{P} C_{4j} Z_{t-j} + \varepsilon_{4t} \qquad (13)$$

$$Y_t = \sum_{j=1}^{P} d_{4j} X_{t-j} + \sum_{j=1}^{P} e_{4j} Y_{t-j} + \sum_{j=1}^{P} g_{4j} Z_{t-j} + \eta_{4t} \qquad (14)$$

$$Z_t = \sum_{j=1}^{P} \mu_{4j} X_{t-j} + \sum_{j=1}^{P} \upsilon_{4j} Y_{t-j} + \sum_{j=1}^{P} \omega_{4j} Z_{t-j} + \gamma_{4t} \qquad (15)$$

and the noise covariance matrix for the above system can be represented as:

$$\Sigma 3 = \begin{pmatrix} var(\varepsilon_{4t}) & cov(\varepsilon_{4t}, \eta_{4t}) & cov(\varepsilon_{4t}, \gamma_{4t}) \\ cov(\eta_{4t}, \varepsilon_{4t}) & var(\eta_{4t}) & cov(\eta_{4t}, \gamma_{4t}) \\ cov(\gamma_{4t}, \varepsilon_{4t}) & cov(\gamma_{4t}, \eta_{4t}) & var(\gamma_{4t}) \end{pmatrix} (16)$$

From these two sets of equations, we define the conditional Granger causality from time series Y_t to X_t conditional on time series Z_t as:

$$F_{X \to Y|Z} = \ln \left(\frac{var(\varepsilon_{3t})}{var(\varepsilon_{4t})} \right) \qquad (17)$$

When the causal influence from time series Y_t to X_t is entirely mediated by other time series Z_t, the coefficients b_4 are uniformly zero, and $var(\varepsilon_{3t}) = var(\varepsilon_{4t})$. As such, $F_{Y \to X|Z} = 0$, meaning that there is no causal influence from Y_t to X_t conditioned on the other time series Z_t. If all the other information included in Z_t is lost, then only pairwise Granger causality between X_t and Y_t can be calculated. On the contrary, when a direct influence from time series Y_t to X_t exists, the inclusion of past measurements of time series Y_t in addition to that of time series X_t and Z_t should result in better predictions of time series X_t, leading to $var(\varepsilon_{3t}) > var(\varepsilon_{4t})$ and $F_{Y \to X|Z} > 0$.

Recent several studies applied Granger causality model on fMRI data in either time[21,22] or the spectral[11,23] domain to investigate the direct causality among different activated brain regions[17,24,25] and within resting state networks.[26,27]

The classical pairwise Granger causality approaches have been widely used in previous fMRI studies. However, the pairwise Granger causality approaches do not clearly distinguish between direct causal influences between one brain region and another and indirect influences from a third factor, also the multivariate causality relationships are difficult to interpret and compare across subjects in group analysis. This could lead to erroneous conclusions about the relationships between regions in fMRI studies.[27] Conditional Granger causality is extremely useful because repeated pairwise analyses among multiple variables can sometimes give misleading results. Another instance in which conditional Granger causality is valuable is when a single source drives two outputs with different time delays.

In recent study, Jiao et al.[28] used pairwise Granger causality approach to investigate the directionality and strength of causal influence between the seven cortical regions within the default mode network (DMN). While in Zhou et al.[27] used conditional Granger causality approach to evaluate both the connectivity and conditional causal influences between four brain Regions of Interest (ROIs) within the DMN and the relationship among resting state networks.

Phase slope index

A recent advancement in the study of signal connectivity is the analysis of Phase Slope Index (PSI) which measures how one signal depends on another, which gives an indication of information flow in complex systems.[29,30] The idea behind the PSI is that the phase of the cross spectrum between two different source activities depends on the time needed for the information to flow between those areas. Thus the derivative of the phase with respect to the frequency, called the phase slope, is proportional to the time needed for the information flow. Therefore, the sign of the phase slope indicates the direction of the information flow. Phase slope index is related to the slope of the phase of the cross spectra between two time series. Large positive values indicate high information outflow and large negative values indicate high information inflow. PSI is the weighted sum of the phase slope of the cross spectrum. The cross spectrum between voxels i and j is defined as:

$$P_{ij}(f) = \langle \sigma_i(f)\sigma_j^*(f) \rangle \qquad (18)$$

Where $\sigma_i(f)$, $\sigma_j(f)$ are the Fourier transform, at frequency (f), of the reconstructed time course at the i voxel and j voxels, respectively. $<.>$ denotes the expectation value which is typically approximated by an average over the segments or trials and * means complex conjugation. The derivative of the phase with respect to the frequency, called the 'phase slope', is proportional to the time needed for the information flow.

Coherency of voxels time series i and j is defined as the normalized crosss-pectrum:

$$C_{ij}(f) = \frac{P_{ij}(f)}{(P_{ii}(f)P_{jj}(f))^{1/2}} \qquad (19)$$

Where P_{ii}, P_{jj} are the power spectrum of i and j respectively. From the magnitude component of coherency, we derive coherence, which is a measure of the linear association between two time series. The coherence is superior to correlation because correlation is sensitive to shape and temporal shift differences in the hemodynamic response, while coherence is invariant in these differences.

The PSI estimates the causal structure between any two source activities. It is defined as:[29]

$$\widetilde{\psi}_{ij} = \text{Im} \left(\sum_{f \in F} C_{ij}^*(f) C_{ij}(f + \delta f) \right) \qquad (20)$$

Where δf is the frequency resolution of the coherency and Im(.) denotes taking the imaginary part.

To see that the definition of $\widetilde{\psi}_{ij}$ corresponds to a meaningful estimate of the average slope it is convenient to rewrite it as:

$$\widetilde{\psi}_{ij} = \sum_{f \in F} \alpha_{ij}(f)\alpha_{ij}(f + \delta f)\sin(\varphi(f + \delta f) - \varphi(f)) \quad (21)$$

Where $C_{ij}(f) = \alpha_{ij}(f)\exp(i\phi(f))$ and $\alpha_{ij}(f) = |C_{ij}(f)|$ being frequency dependent weights. For smooth phase spectra $\sin(\phi(f+\delta f)-\phi(f)) \approx \phi(f +\delta f)-\phi(f)$, and hence $\widetilde{\psi}$ corresponds to a weighted average of the slope.

It is convenient to normalize $\widetilde{\psi}$ by an estimate of its standard deviation:

$$\psi = \frac{\widetilde{\psi}}{std(\widetilde{\psi})} \quad (22)$$

With $std(\widetilde{\psi})$ being estimated by the Jackknife method. We compute ψ using the MATLAB software available at.[29]

Resting-state functional connectivity MRI (fc-MRI) uses task-free blood oxygenation level dependent (BOLD) time courses to measure the temporal correlation between different regions of the brain. The aim of this study is to compare between Granger causality and Phase Slope Index to explain fMRI resting state time series causality.

METHODS

Imaging methods

Fourteen healthy right-handed volunteers (mean age [SD] = 29.2[4.6] yrs; 5 female) were recruited for this study. Volunteers were excluded if they had any medical, neurological, or psychiatric disease. All participants gave written informed consent. During the resting experiment the scanner room was darkened; subjects were lying supine in the MRI scanner and were instructed to rest quietly but alert keeping their eyes open and looking at a fixation crosshair presented in the center of the subjects field of view to limit eye movements and to stay awake at all times. Throughout the entire scanning session subjects were instructed to think of nothing in particular.

Resting state fMRI data were acquired on a 3T system (GE HDx). Functional data were collected by using a 2D gradient echo planar sequence, sensitive to Blood Oxygen Level Dependent (BOLD) contrast, with repetition time (TR): 3000 ms; echo time (TE): 35 ms; number of slices: 53 (interleaved); slice thickness: 3.2 mm; matrix size: 64x64; flip angle: 90°; in-plane resolution: 3.2x3.2 mm^2. A total of 125 functional images were acquired with the subjects in the resting condition, corresponding to a total imaging time of 6 min and 25 sec. Subsequently, a T1 weighted structural scan was also acquired, (1x 1x 1 mm^3), to provide the anatomical reference.

Data analysis

Image preprocessing and statistical inference were carried out using statistical parametric mapping (SPM8) software package (http://www.fil.ion.ucl.ac.uk/spm/) and homemade developed software realized in MATLAB. The physiological noise fluctuations were corrected using RETROICOR,[31] while low frequency respiratory and heart rate effects were removed by using RVHRCOR.[32] Images of the first five scans were discarded before further processing to make sure that the MR signal had reached steady state.

Several processing steps were used to optimize the voxel-wise analysis. Sources of spurious variance were removed from data by means of linear regression of six parameters (three translations and three rotations) obtained by rigid body correction of head motion. Most data analysis schemes assume that every voxel was sampled at exactly the same time. Slice acquisition correction compensates for staggered order of slice acquisition. Data were temporally band pass filtered (0.009Hz < f < 0.15Hz). In the final step of the preprocessing pipeline, the data were spatial smoothed with an isotropic Gaussian kernel of 8 mm full-width half-maximum [FWHM]; this is indeed a common practice to digitally smooth fMRI data in space prior to statistical analysis.

Regions of interest

We selected seed regions of interest in the Posterior Cingulate Cortex (PCC) with 8 mm radius sphere centered at (0,-46,32) in Montreal Neurological Institute (MNI) space, then excluding uninteresting signals by intersection the PCC voxels and gray matter (GM) mask to select the interest voxels. The ROI was defined in MNI space and reverse normalized to each subject's mean functional image using SPM8.

For each subject, the mean time series across all voxels in the ROI was extracted, and the correlation coefficient was computed with the time series of every voxel in the brain. Single subject correlation maps were converted to Fisher Z-statistics prior to group analysis. Group maps of the DMN were computed by normalizing Fisher Z-transformed correlation maps to a standard template and entering them into a random-effects analysis using SPM8.

The coordinates of the highest activating voxel are then used to define a seed voxel in the resting data. Within each masked region, ROIs were identified as the most significant voxel and all surrounding significant voxels within 8 mm radius.

Granger causality mapping

The technique of fMRI Granger causality mapping explores all regions in the brain that interact with a single selected reference region using Granger causality as a

measure of directed influence or information flow. Granger causality analyses were performed as described in Roebroeck et al.[16] By employing a simple bivariate model containing the reference region and, in turn, every other GM voxel, the sources and targets of influence for the reference region can be mapped. We computed the pairwise Granger causality between time series of reference region and GM voxels. When performing simultaneous statistical tests for all voxels, we assessed the significance thresholds by correcting for multiple comparisons using the false discovery rate (FDR).

A critical element in the specification of vector autoregressive (VAR) models is the determination of the lag length of the VAR. Various lag length selection criteria are defined by different authors like, Akaike's (1969) final prediction error (FPE), Akaike Information Criterion (AIC) suggested by Akaike (1974), Schwarz Criterion (SC) (1978) and Hannan-Quinn Information Criterion (HQ) (1979).

In the current study, the optimal order for the fMRI data is selected following Akaike Information Criterion (AIC). The input of the Granger causality analysis consisted of the average time series of the reference region and the time series of GM voxels. For each reference region, we created four different maps:

1. Reference to voxel map ($F_{R \to V}$),
2. Voxel to Reference map ($F_{V \to R}$),
3. Instantaneous influence map ($F_{V.R}$), and
4. Influence difference map ($dF_{V.R} = F_{R \to V} - F_{V \to R}$).

The two directions of Granger causality, ($F_{R \to V}$ and $F_{R \to V}$), are subtracted from each other to generate differential Granger causality maps, such that positive values indicate more Granger causality from the reference to the brain's voxel than from the brain's voxel to the reference region. For a particular pattern, each Granger map was entered into a second-level random effects analysis and assessed statistically.

PSI mapping

The PSI computes a directed, pairwise measure of interaction between two time series using the cross-spectrum. To identify the resting state information flows, we generated PSI maps by computing PSI values between a reference seed time series and all GM voxels. All calculations were done in MATLAB R2007b (The MathWorks Inc., Natick MA), the script calculating PSI used in this study has been published previously.[29] Because in resting state the hemodynamic response function only has a power in the low frequency band, we focus our analysis on the 0.009 - 0.1 Hz band.

As the described above, the averaged BOLD response time course of voxels in reference region was considered as the time series i. Subsequently, the BOLD response time series of each single voxel in the functional volume

was taken as the time series j and PSI(i, j) were computed. This measure is normalized by its standard deviation to to determine whether causal influence between I and j is significant.

In general, if PSI(i, j) has a positive value, the information flows from the i voxel to the j voxel locations (from Ref-Voxel), and if the PSI(i, j) has a negative value, the information flows from the j voxel to the i voxel (from Voxel-Ref). The PSI maps were computed for each ROI. To increase the frequency resolution and to estimate PSI in low frequency range, we concatenate multiple brain volumes across the subjects into a single data set. The order of the subject volumes was counterbalanced across the concatenated multiple brain volumes. We defined the GM common mask in MNI space, to compute the PSI between reference regions and brain voxels.

Finally, second-level analysis (one sample t-test) was carried out, where PSI maps from several subjects are pooled and then thresholded, in order to determine the brain areas that show significant positive and negative PSI values.

RESULTS

Regions of interest

The z-maps were computed from resting data for each subject then transformed to MNI common space. A t-test was performed on each pixel of these maps (using the data across all subjects) to produce a composite map of the statistical significance of resting state correlations with PCC. Figure 1 shows the group level statistical maps appear superimposed on the render template brain from the MRIcro software (http://www.mricro.com). To select and define the ROIs, we identified the regions that are most strongly positive correlation with the PCC (for regions, Brodmann Areas (BA) and coordinates, see Table 1). These ROIs were located in Medial Prefrontal Cortex (MPFC), Left Lateral Parietal Cortex (LLPC), and Right Lateral Parietal Cortex (RLPC).
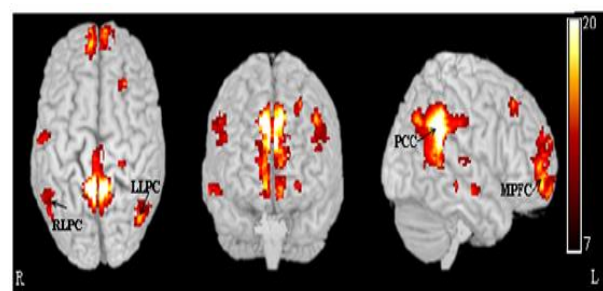

Figure 1: Group-level thresholded t-maps for positive correlations with the PCC.

Table 1: Brain regions that correlated positively with the PCC during resting.

Regions	Abbreviations	BA	Coordinates
Posterior Cingulate Cortex	PCC	23/30	-2,-46,28
Medial Prefrontal Cortex (ventral)	MPFC	10/11	5,55,-12
Left Lateral Parietal Cortex	LLPC	39	-47,-66,32
Right Lateral Parietal Cortex	RLPC	39	48,61,29

Granger causality

The technique of Granger Causality Mapping was developed to explore all regions in the brain that interact with a single selected reference region using autoregressive modelling of fMRI time series. The autoregressive order used for the computation of the influence measured was set to 5, as suggested by the order selection criteria. For each reference regions (PCC, MPFC, RLPC, and LLPC), we computed the bivariate Granger causality maps.
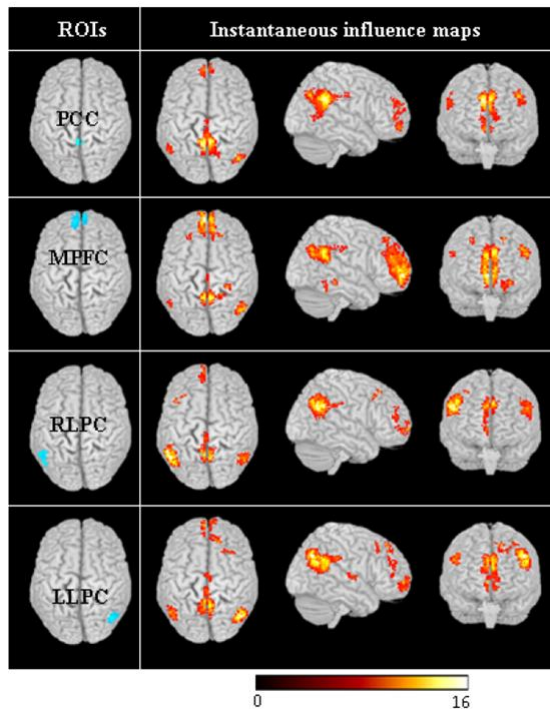
Figure 2: The instantaneous influence maps for each region of interest.

The resulting instantaneous influence maps ($F_{V.R}$) are shown in figure 2 separately for each region of interest. The left side represents the reference regions and the right side represents the undirected instantaneous influence maps for each reference region. The instantaneous influence maps were entered into a second-level random-effects analysis and thresholded at P<0.001 uncorrected, with an extent threshold of 10 voxels. The instantaneous influence term essentially quantifies partial correlation (functional connectivity) that cannot be assigned to influence in a certain direction purely from temporal information in the data. So the instantaneous influence term of the Granger causality can be seen to have no direction and may not provide clear evidence for interactions.
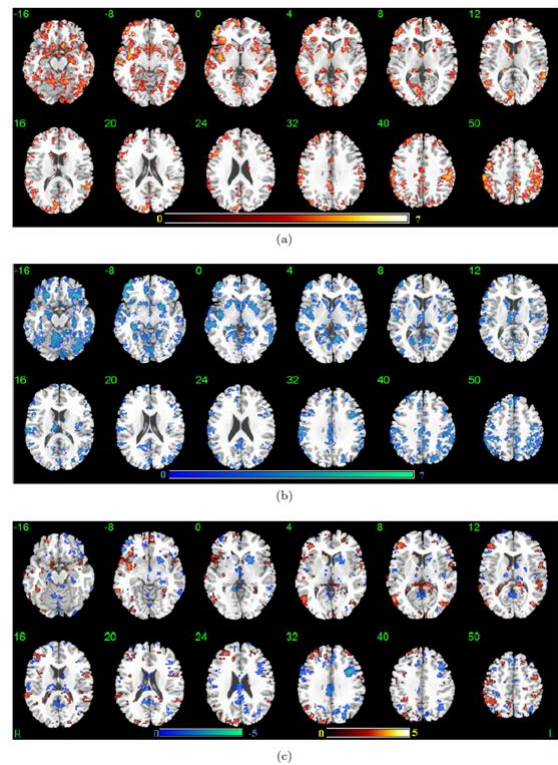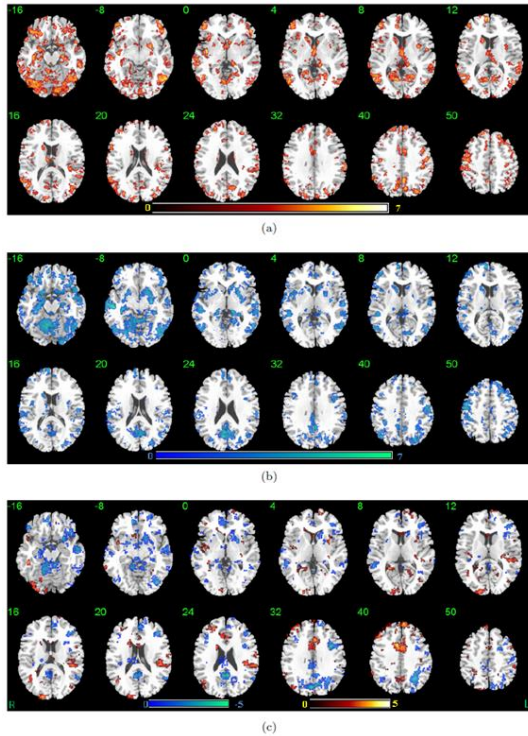

Figure 3: Granger causality map of the regions influenced by the seed PCC, (a) PCC to voxel map ($F_{R \rightarrow V}$), (b) Voxel to PCC map ($F_{V \rightarrow R}$), and (c) influence difference map ($dF_{V.R}$).

Figure 3 shows three influence maps, (a) PCC to voxel map ($F_{R \rightarrow V}$), p <0.005 uncorrected, showing voxels which are influenced by the activity in the PCC seed, (b) Voxel to PCC map ($F_{V \rightarrow R}$), p <0.005 uncorrected, showing voxels whose activity influence the activation in the PCC seed, and (c) Influence difference map ($dF_{V.R}$), p <0.05 uncorrected. The difference map demonstrate two directions: influence from the reference region PCC to GM voxels is shown in red-yellow color scale (red color indicate low, and yellow color represent high, values across subjects), and influence from GM voxels to the reference region PCC is shown in blue-green color scale

(blue colors indicate low, and green colors represent high, values across subjects).

In the influence difference map ($dF_{V.R} = F_{R \to V} - F_{V \to R}$) in figure 3(c), the regions RLPC (BA. 39), LLPC (BA. 39), calcarine (BA. 17), hippocampus (BA. 27), and ventral medial prefrontal cortex vMPFC (BA. 10) are showing the increases in influence values from the seed PCC. The regions that show increase in influence values into the PCC seed include: cuneus (BA. 18, NA), thalamus (BA. NA), cerebellum (BA. 18, 19), LLPC (BA. 39) and dorsal medial prefrontal cortex dMPFC (BA. 9, 32).
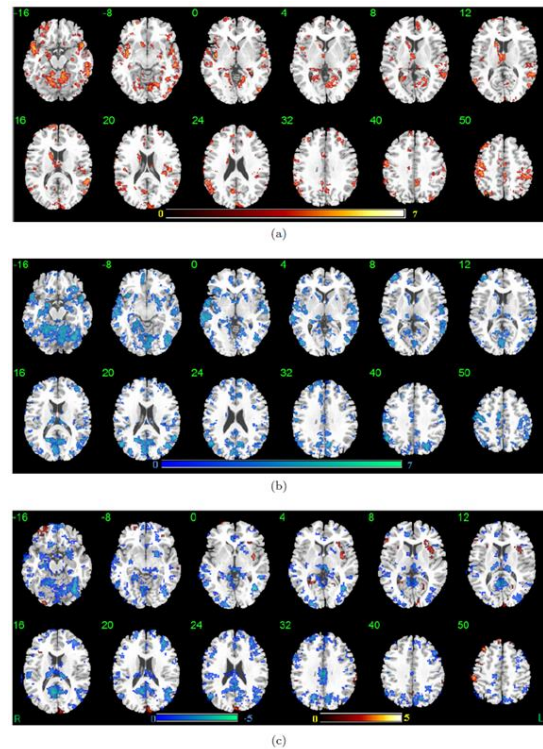

Figure 4: Granger causality map of the regions influenced by the seed MPFC, (a) MPFC to voxel map ($F_{R \to V}$), (b) voxel to MPFC map ($F_{V \to R}$) and (c) influence difference map ($dF_{V.R}$).

In figure 4 we display three Granger causality sub-maps: (a) MPFC to voxel map, (b) Voxel to MPFC map, and (c) Influence difference map. From the influence difference map, we find that the significant causal influences from the MPFC seed to calcarine (BA. 17), cerebellum (BA. 18, 19), RLPC (BA. 39), LLPC (BA. 39), precuneus (BA. 23), and thalamus (BA. NA). The regions show significant causal influences into the MPFC seed are PCC (BA. 23), hippocampus (BA. 27), cerebellum (BA. 18, 19), thalamus (BA. NA) and cuneus (BA. 18, NA).

The significant causality was observed from the RLPC represented in figure 5, (a) RLPC to voxel map, p <0.005 uncorrected, (b) Voxel to RLPC map, p <0.005 uncorrected, and (c) Influence difference map, p <0.05 uncorrected. We can note that, small significant causal influences for RLPC into GM voxels. The significant

causal influences from GM voxels into RLPC seed are most pronounced than the significant causal influences from RLPC into GM voxels.

In the RLPC influence difference map figure 5(c), shows the direction of causality form RLPC into calcarine (BA. 17). The regions cuneus (BA. 18, NA), PCC(BA. 23), hippocampus (BA. 27), LLPC (BA. 39), dMPFC (BA. 9,32), vMPFC (BA. 10), thalamus (BA. NA), and hippocampus (BA. 27) shows the direction of causality into RLPC seed.

Figure 5: Granger causality map of the regions influenced by the seed RLPC, (a) RLPC to voxel map ($F_{R \to V}$), (b) voxel to RLPC map ($F_{V \to R}$) and (c) influence difference map ($dF_{V.R}$).
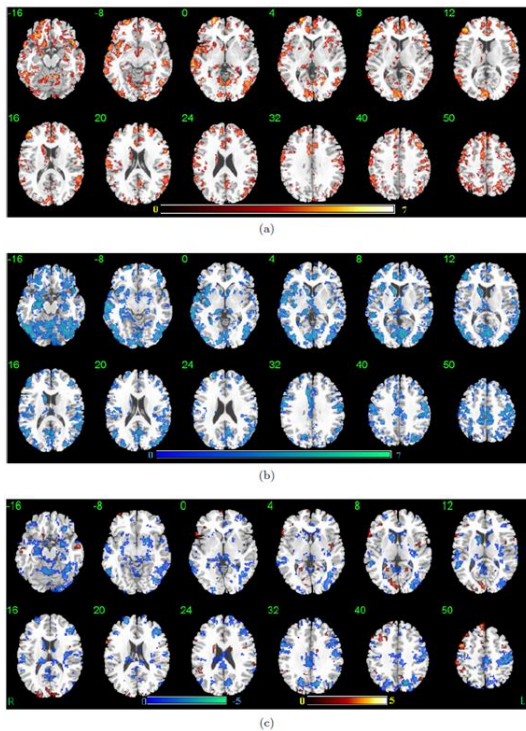
Figure 6 shows the LLPC to voxel maps, voxel to LLPC map, and influence difference map, thresholded at P <0.001 uncorrected. The influence difference map shows the significant causal influences from and into LLPC seed. We can note the significant causal influences from LLPC to the calcarine (BA. 17), RLPC (BA. 39), and vMPFC (BA. 10). The causal flow from PCC (BA. 23), thalamus (BA.NA), hippocampus (BA. 27), cuneus (BA. 18, NA) and cerebellum (BA. 18, 19) into LLPC seed.

To summarize, the significant causal influences for the two directions (in and out) between GM voxels and reference regions (PCC, MPFC, RLPC, and LLPC) are represented in figure 7. The blue arrows highlight the causal flow from the GM voxels into the reference regions, while the red arrows highlight the causal flow form reference regions into the voxels.

Slope phase index

This section presents results of our experiments on estimating the directions of information flow between resting state activity regions. We applied the source PSI analysis to resting state fMRI data, PSI estimated in the range from 0.01Hz into 0.1 Hz. We computed the PSI between GM voxel and different four ROIs (PCC, MPFC, RLPC and LLPC).
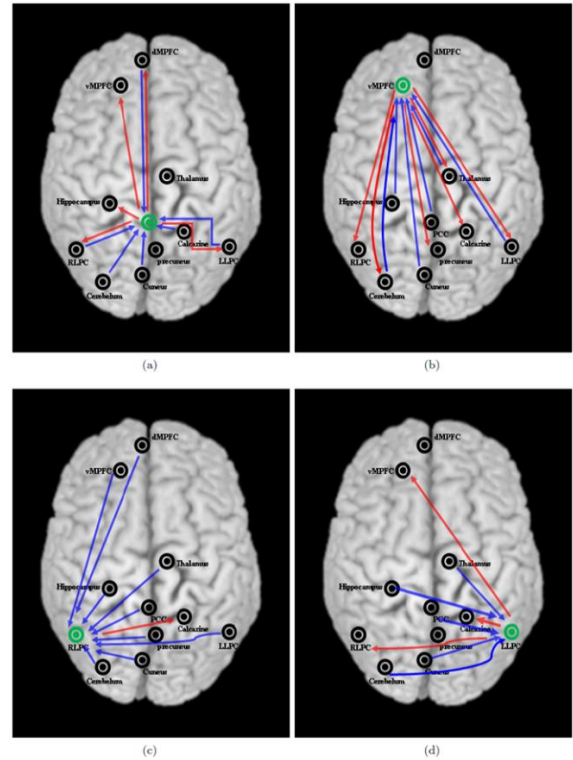
In our results, the positive PSI values indicate the direction of the information flow from the reference region into the GM voxels, while the negative PSI values indicate the direction of the information flow from the GM voxels into seed reference region.

Figure 7: The direction of the Granger causality influence between GM voxelsand (a) PCC, (b) MPFC, (c) RLPC and (d) LLPC.

In these results, the different regions with positive and negative values are clearly detected, and the results suggest that there is an information inflow and information outflow between PCC and GM voxels. Figure 8 shows the information outflow from PCC reference region into vMPFC (BA. 10), hippocampus (BA. 27), cerebellum (BA. 18, 19), and precuneus (BA. 23). On the other hand, this figure shows the information inflow from calcarine (BA. 17), RLPC (BA. 39), LLPC (BA. 39), dMPFC (BA. 9, 32), precuneus (BA. 23) and thalamus (BA. NA) into the PCC reference region.

Figure 6: Granger causality map of the regions influenced by the seed LLPC, (a) LLPC to voxel map ($F_{R \to V}$), (b) voxel to LLPC map ($F_{V \to R}$) and (c) influence difference map ($dF_{V.R}$).
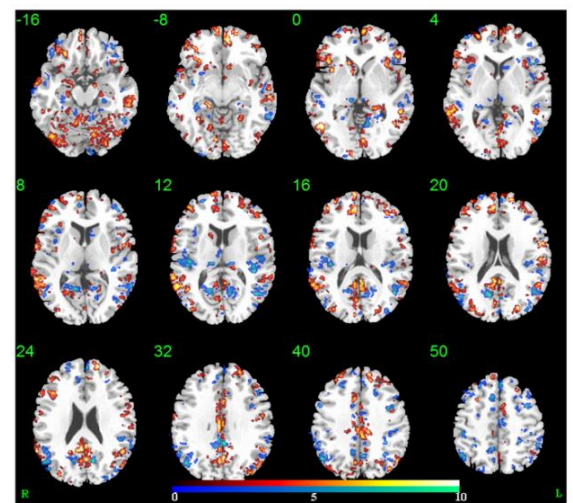
One sample t-tests in SPM8 were used to assess the statistical significance of each identified PSI pattern. For a particular pattern, PSI map was entered into a second-level random-effects analysis and assessed statistically using a threshold of P <0.001 uncorrected and minimum cluster size of >10 contiguous voxels.

The positive and negative PSI map between PCC and GM voxels are shown in figure 8. The red color scale refers to the voxels that have the positive PSI with the PCC ROI, while the blue color scale refers to the negative PSI value. All PSI maps were thresholded at P <0.001 uncorrected (one-sample t-test).


Figure 8: PSI map for PCC seed.

The information flow from the reference region MPFC and GM voxels are shown in figure 9. The positive and negative PSI values were thresholded at P <0.001 uncorrected and with an extent threshold of 10 voxels. The regions of information inflow and information outflow between MPFC and GM voxels are clearly detected. Figure 9 shows the positive and negative flux between MPFC and GM voxels. As shown in this figure, the information outflow from MPFC into RLPC (BA. 39), LLPC (BA. 39), thalamus (BA. NA), hippocampus (BA. 27) and cerebellum (BA. 18, 19). The information inflow regions are PCC (BA. 23), precuneus (BA. 23), calcarine (BA. 17), cuneus (BA. 18, NA).
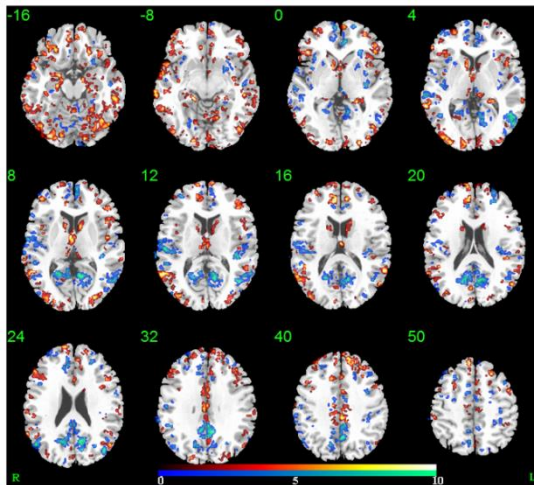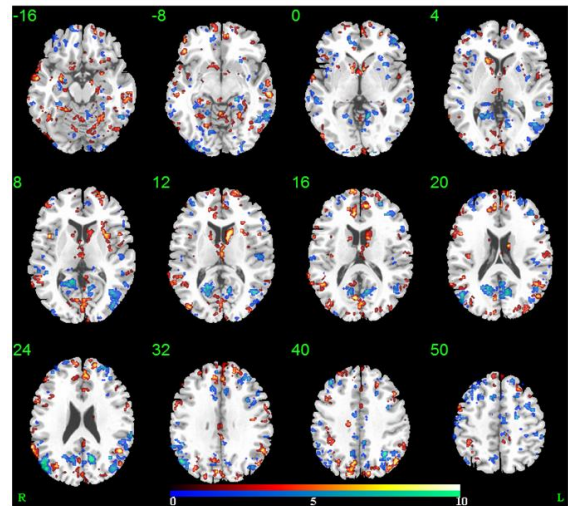

Figure 9: PSI map for MPFC seed.

The results of mapping of PSI values between RLPC reference region and GM voxels are shown in figure 10. We can note that, the positive PSI regions are more pronounced than the negative PSI regions. Figure 10 shows the direction for information outflow and information inflow between RLPC reference region and GM voxels. The positive PSI region which represent the information outflow are PCC (BA. 23), LLPC (BA. 39), precuneus (BA. 23), dMPFC (BA. 9, 32), cerebellum (BA. 18, 19), hippocampus (BA. 27), and thalamus (BA. NA). The regions of information inflow are vMPFC (BA. 10), hippocampus (BA. 27), and thalamus (BA. NA).
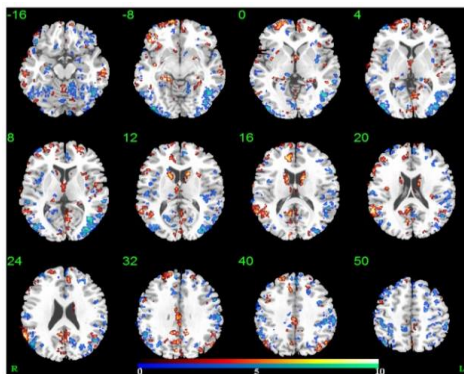

Figure 10: PSI map for RLPC seed.

Results of second-level of PSI mapping between LLPC reference region and GM voxels are shown in figure 11. PSI map is statistically thresholded at P <0.001 uncorrected for multiple comparisons and minimum cluster size of >10 contiguous voxels. Figure 11 showing voxels which are received information from LLPC, these regions include vMPFC (BA. 10), dMPFC (BA. 9, 32), hippocampus (BA. 27), and thalamus (BA. NA). The regions of information inflow are PCC (BA. 23), RLPC (BA. 39), and calcarine (BA. 17).

Figure 11: PSI map for LLPC seed.
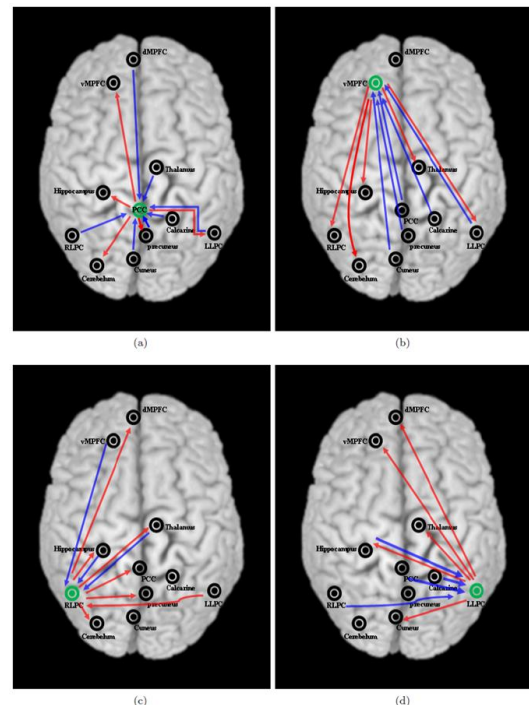
Figure 12: The direction of the PSI information inflow (blue arrows) and outflow (red arrows) between GM voxels and (a) PCC, (b) MPFC, (c) RLPC and (d) LLPC.

Figure 12 shows the causal direction between the reference regions (PCC, MPFC, RLPC, and LLPC) and GM voxels. Red arrows highlight the direction of information flow from the reference regions seed into the voxels (positive PSI values) and the blue arrows highlight the direction of information flow from GM voxels into reference regions (negative PSI values).

DISCUSSION

In the present study, we introduced two different approaches to investigate the information flow between the resting state regions. The approaches are Granger causality and the slope phase index. The technique of Granger causality Mapping was developed to explore all regions in the brain that interact with a single selected reference region using autoregressive modeling of fMRI time series. Granger causality maps for four components: $F_{R \rightarrow V}$, $F_{V \rightarrow R}$, $F_{V.R}$, and $dF_{V.R} = F_{R \rightarrow V} - F_{V \rightarrow R}$ were calculated by Matlab software.

The newly Phase Slope Index (PSI) is a measure of how one time series depends on another, which gives an indication of information flow in complex systems. We applied the PSI analysis to resting state fMRI data to direction of information flow between DMN regions. The PSI computed between the average reference region time series and GM voxels time series. For each reference region, we created PSI maps and then performed a second-level random effects analysis to create the significant positive and negative PSI maps.

We applied Granger causality and PSI mapping for four DMN reference regions are PCC, MPFC, RLPC, and LLPC. Based on our results, we can note that similar patterns can be seen for some reference regions (e.g. PCC) and a significant difference between the two approaches for other reference regions (e.g. RLPC). Now, we compare between two approaches for each reference region.

For PCC seed, the results for Granger causality and PSI patterns are shown in figure 3 and figure 8. The direction of interactions between PCC seed and GM voxels in group level for Granger Causality and PSI are shown in figure 7(a) and figure 12(a). For Granger causality and PSI, PCC seed has a strong directional influence upon the vMPFC, hippocampus and LLPC. The brain regions, RLPC, LLPC, thalamus, cuneus, and dMPFC show significant influence on PCC seed for the two approaches. These results indicate that, the two approaches explore the same influence direction for PCC reference region and brain regions. On the other hand, we can note some difference between the two approaches. The bidirectional (inflow and outflow) influence between the PCC seed and brain regions dMPFC and RLPC is detected only by Granger causality. For PSI approach, we can note only inflow influence from dMPFC and RLPC into PCC seed is in agreement with the findings in the previous studies using various approaches.[28,27]

For MPFC seed, the Granger causality and PSI mapping results are shown in Figure 4 and Figure 9. The direction of interactions between MPFC seed and GM voxels for Granger causality and PSI are shown in Figure 7(b) and Figure 12(b). The direction of influence from the MPFC seed into RLPC, LLPC, and thalamus are detected in PSI and Granger causality approaches. The influence from cuneus, LLPC, and PCC into MPFC seed are detected in the two approaches. The bidirectional influence between MPFC seed and thalamus and cerebellum are detected only in Granger causality mapping. The influence directions for hippocampus, precuneus, and calcarine with MPFC for PSI mapping reverse the directions for Granger causality mapping.

For RLPC seed, the Granger causality and PSI mapping results are shown in Figure 5 and Figure 10. The direction of interactions between RLPC seed and GM voxels in group level for Granger causality and PSI are shown in Figure 7(c) and Figure 12(c). We can note the significant difference in the influence from RLPC seed into GM voxels between PSI and Granger causality approaches. In PSI and Granger causality, the same directions of influence from vMPFC, thalamus, and hippocampus into RLPC are detected in the two approaches. The influence of Granger causality is the reverse of PSI influence between RLPC and PCC, dMPFC, precuneus, cerebellum and LLPC regions. In general, based on our results the PSI mapping is more accurate than Granger causality mapping because the RLPC has been showing outflow information more than in flow information.[27]

Finally, for LLPC seed the results for Granger causality and PSI patterns are shown in Figure 6 and Figure 11. The direction of interactions between PCC seed and GM voxels in group level for Granger Causality and PSI are shown in Figure 7(d) and Figure 12(d). The influence between the LLPC seed and vMPFC, PCC, and hippocampus are detected in PSI and Granger causality mapping. The influence of Granger causality is reverse PSI influence between LLPC seed and cuneus, thalamus, RLPC and calcarine. The influence between dMPFC, and hippocampus are detected only in PSI mapping.

In this study, we compare pair wise Granger causality and PSI approaches and interpret results of both methods which apply on the same resting state fMRI data set. Granger causality based on multivariate autoregressive models has been used to analyse directions of information flow in multi-channel time series. On the other hand, PSI approach evaluates a slope of a phase of cross spectra between two fMRI time series and behaves better than Granger causality in noisy conditions. In some cases Granger causality gives fake albeit significant results. Granger causality has a tendency to detect causal connections even in the case when they are not present. PSI is insensitive to mixture of independent sources, gives meaningful results even if the phase spectrum is not

linear, and properly weights contributions from different frequencies.

The final fMRI signal arises from a complex chain of processes that we can classify into neuronal, physiological and physical processes,[33] each of which contain some crucial parameters and variables and have been modelled in various ways. The problem is particularly important in fMRI time series: A certain area X can cause a response in another area Y through neuronal activity, but the hemodynamic responses in X might appear much later than those in Y. This would imply that Y Granger-caused X. On the other hand, it is important to eliminate spurious causalities that may appear when time series are both influenced by the other external sources that are not taken into account from the Granger causality analysis.

It is well known that a pairwise evaluation for multivariate data has the limits that one cannot discern whether the influence between two time series is direct or is mediated by the other.[34] The classical pairwise Granger causality approaches have been widely used in previous fMRI studies. However, the pairwise Granger causality mapping approaches do not clearly distinguish between direct causal influences between one brain region and another indirect influences from a third factor, also the multivariate causality relationships are difficult to interpret and compare across subjects in group analysis. This could lead to erroneous conclusions about the relationships between regions in fMRI studies.[27]

To conclude, the PSI based approach is non-parametric and has several advantages over parametric approaches such as multivariable autoregressive models, which are used to compute Granger causality, directed transfer functions, and partially directed coherence. We showed that the Granger causality and PSI mapping for fMRI resting state data set. The PSI approach proposed herein is effective, computationally efficient, and easy to interpret. We note that, PSI influence directions between reference regions and GM voxels were consistent more than Granger causality with the previous results.

ACKNOWLEDGEMENTS

REFERENCES

1. Granger CW. Investigating causal relations by econometric models and cross spectral methods. Econometrica. 1969;37:424-38.
2. McIntosh AR. Understanding neural interactions in learning and memory using functional neuroimaging. Ann. NY Acad. Sci. 1998;8:556-71.
3. Friston KJ, Harrison L, Penny W. Dynamic causal modelling. Neuroimage. 2003;19:1273-1302.
4. Wiener N. The theory of prediction. In: E. F. Beckenbach, Eds. Modern Mathermatics for Engineers. 1st ed. New York: McGraw-Hill; 1956: 177.
5. Wayne J. Economic growth and defence spending: Granger causality. J. Dev. Econ. 1986;21:35-40.
6. Hiemstra C, Jones JD. Testing for linear and nonlinear granger causality in the stock price volume relation. J. Finance. 1994;49:1639-64.
7. Fujita A, Sato JR, Garay-Malpartida H, Sogayar MC, Ferreira CE, Miyano S. Modelling nonlinear gene regulatory networks from time series gene expression data. J. Bioinform. Compute. Biol. 2008;6:961-79.
8. Fujita A, Sato JR, Ferreira CE, Sogayar MC. Gedi: a user-friendly toolbox for analysis of large-scale gene expression data. BMC Bioinform.2007;8:457.
9. Kaufmann R. K, D'Arrigo RD, Laskowski C, Myneni R. B, Zhou L, Davi NK. The effect of growing season and summer greenness on northern forests. geophys. Res. Lett. 2004;31:L09205.
10. Elsner JB. Evidence in support of the climate change-atlantic hurricane hypothesis. Geophys. Res. Lett. 2006;33:L16705.
11. Sato JR, Takahashi YD, M.Arcuri S, Sameshima K, Morettin PA, Baccal LA. Frequency domain connectivity identification: an application of partial directed coherence in fmri. Hum. Brain Mapp. 2009;30:452-61.
12. Schelter B, Timmer J, Eichler M. Assessing the strength of directed influences among neural signals using renormalized partial directed coherence. J. Neurosci. Meth. 2009;179:121-30.
13. Hemmelmann D, Ungureanu M, Hesse W, Wstenberg T, Reichenbach JR, Witte OW, Witte H, Leistritz L. Modelling and analysis of time-variant directed interrelations between brain regions based on bold-signals. Neuroimage. 2009;45:722-37.
14. Abler B, Roebroeck A, Goebel R, Hose A, Schfnfeldt-Lecuona C, Hole G, Walter H. Investigating directed influences between activated brain areas in a motorresponse task using fMRI. Magn. Reson. Imaging 2006;24:181-5.
15. Goebel R, Roebroeck A, Kim DS, Formisano E. Investigating directed cortical interactions in time-resolved fMRI data using vector autoregressive modelling and Granger causality mapping. Magn. Reson. Imaging. 2003;21:1251-61.
16. Roebroeck A, Formisano E, Goebel R. Mapping directed influence over the brainusing granger causality and fMRI. Neuroimage. 2005;25:230-42.

17. Liao W, Mantini D, Zhang Z, Pan Z, Ding J, Gong Q, Yang Y, Chen H. Evaluating the effective connectivity of resting state networks using conditional Granger causality. Biol. Cybern. 2010;102:57-69.
18. Michael CS, Godfrey DP, Vince DC. Changes in the interaction of resting-stateneural networks from adolescence to adulthood. Hum. Brain Mapp. 2009;30:2356-66.
19. Zhou Z, Chen Y, Ding M, Wright P, Lu Z, Liu Y. Analysing brain networks with PCA and conditional Granger causality. Hum. Brain. Mapp. 2009;30:2197-2206.
20. Chen Y, Bressler SL, Ding M. Frequency decomposition of conditional Granger causality and application to multivariate neural field potential data. J Neurosci Meth-ods. 2006;150:228-37.
21. Kayser AS, Sun FT, D'Esposito M. A comparison of granger causality and coherency in fMRI-based analysis of the motor system. Hum Brain Mapp. 2009;30:3475-94.
22. Londei A, D'Ausilio A, Basso D, Belardinelli MO. A new method for detecting causality in fMRI data of cognitive processing. Cogn. Process. 2006;7:42-52.
23. Demirci O, Stevens MC, Andreasen NC, Michael A, Liu J, White T, Pearlson GD, Clark VP, Calhoun VD. Investigation of relationships between fmribrain networks in the spectral domain using ICA and Granger causality reveals distinct differences between schizophrenia patients and healthy controls. Neuroimage. 2009;46:419-31.
24. Sato JR, Junior EA, Takahashi DY, de Maria Felix M, Brammer MJ, Morettin PA. A method to produce evolving functional connectivity maps during the course of an fMRI experiment using wavelet-based time varying Granger causality. Neuroimage. 2006;31:187-96.
25. Duann JR, Ide JS, Luo X, Li CS. Functional connectivity delineates distinct roles of the inferior frontal cortex and pre-supplementary motor area in stop signal inhibition. J. Neurosci. 2009;29:10171-9.
26. Uddin LQ, Kelly AM, Biswal BB, Castellanos FX, Milham MP. Functional connectivity of default mode network components correlation, anti-correlation and causality. Hum Brain Mapp. 2009;30:625-37.
27. Zhoua Z,Wanga X, Klahrc NJ, Liua W, Ariasa D,Liua H, von Deneenc KM, Wena Y,Lub Z, Xua D, Liuc T. A conditional Granger causality model approach for group analysis in functional magnetic resonance imaging. Magn. Res. Med. 2011;29:418-33.
28. Jiao Q, Lu G, Zhang Z, Zhong Y, Wang Z, Guo Y, Li K, Ding M, Liu Y. Granger causal influence predicts bold activity levels in the default mode network. Hum. Brain Mapp. 2011;32:154-61.
29. Nolte G, Ziehe A, Nikulin V, Schlgl A, Krmer N, Brismar T, Mller KR. Robustly estimating the flow direction of information in complex physical systems. Phys. Rev. Lett. 2008;100:234101.
30. Nolte G, Ziehe A, Kramer N, Popescu F, Muller KR. Comparison of Granger causality and phase slope index. JMLR Workshop Con. Proc. 2010;6:267-76.
31. Glover GH, Li TQ, Ress D. Image-based method for retrospective correction of physiological motion effects in fMRI: Retroicor. Magn. Reson. Med. 2000;44:162-7.
32. Chang C, Cunningham JP, Glover GH. Influence of heart rate on the bold signal: The cardiac response function. Neuroimage. 2009;44:857-69.
33. Uludag K, Dubowitz DJ, Buxton RB. Basic principles of functional MRI. In R. Edelman, J. Hesselink, and M. Zlatkin, eds. Clinical MRI. San Diego: Elsevier; 2005: 249-287.
34. Kaminski M, Ding M, Truccolo WA, Bressler SL. Evaluating causal relations in neural systems: Granger causality, directed transfer function and statistical assessment of significance. Biol. Cybern. 2001;85:145-57.